ROYAL SOCIETY
OF CHEMISTRY

PAPER

Check for updates

Molecular and histological evidence for the biocompatibility of PEDOT-coated microneedles in human skin†

Siti Musliha Ajmal Mokhtar, [a] Nathalie J Nataren, [b] Drew R Evans, [c] Mark Moore,[d] Samuel Bradley,[e] Sofia MacHacaz Palmar, [e] Tarl W Prow[e] and Miko Yamada*[e]

The increasing demand for real-time, continuous health monitoring has driven improvements in wearable and skin-attachable devices, particularly in sensing vital body signs and biomarkers. Research on conducting polymers (CPs) in these devices is also growing due to their low cost, flexibility, and versatile fabrication. However, despite their widespread use and claims of biocompatibility, there are limited studies on the biocompatibility of CPs in human skin, and those that exist have only been conducted using cell cytotoxicity or animal testing, lacking proper and comprehensive assessments. To address this critical gap, this study investigates the biocompatibility of CPs, represented by poly(3,4-ethylenedioxythiophene) (PEDOT), in excised human skin. In addition to the pathological evaluation of skin biopsies, a novel assessment of CP's impact on the expression of stress-related gene markers is reported, providing a comprehensive analysis at both the tissue and molecular levels. PEDOT-coated microneedles were implanted in the skin for transdermal interrogation, and after 24 hours of incubation, the exposed skin was studied using histology and RT-PCR. This paper offers fundamental insights for future CP-engineered devices in skin applications, contributing valuable data to the materials community regarding the true biocompatibility of these widely used materials.

1 Introduction

In modern healthcare technology, wearable medical devices are increasingly utilized to deliver continuous, real time health information for personalized and accessible healthcare.[1] Commercial wearable devices typically track physical activities, such as step count, and vital body signs, including heart rate and caloric expenditure.[2] However, recent advances in wearable biosensing have expanded beyond basic physiological monitoring to the detection of critical biomarkers related to health conditions,[3] including electrolytes,[4] metabolites,[5,6] hormones,[7] proteins,[8,9] and

oligonucleotides.[10] Amid these breakthroughs, non-invasive sensing in sweat and minimally invasive transdermal sensing in interstitial fluid (ISF) have gained attention as alternatives to conventional blood sampling due to reduced pain,[11] and comparable biomarker concentrations to blood.[10,12,13]

Microneedles (MN)s have emerged as significant devices capable of penetrating the skin barrier to access dermal ISF within the dermis layer.[14,15] Over the past decade, functionalized MNs have been developed for diagnostic and therapeutic applications on the skin.[16] They have also been adapted as electrochemically active electrodes in biosensing, integrating materials such as gold or nanoparticles to enhance performance. Among these advancements, MN-based biosensors integrated with conducting polymers (CPs) offer a promising platform for skin-interfacing applications. Conducting polymers (CP)s, particularly poly(3,4-ethylenedioxythiophene) (PEDOT),[4,17] along with polyaniline (PANI)[18,19] and polypyrrole (Ppy),[20,21] have garnered increasing attention for biomedical applications due to their electrical conductivity and biocompatibility.[22] CPs consist of aromatic rings joined together, forming a π-bonded conjugated backbone with alternating carbon–carbon single and double bonds.[23] Defects within this backbone serve as charge carriers, which are electrostatically stabilized by co-located counterion within the polymer

[a] *College of Engineering, Universiti Teknologi MARA, Johor Branch, Pasir Gudang Campus, Masai, Johor 81750, Malaysia*
[b] *Centre for Cancer Biology, University of South Australia and SA Pathology, Adelaide, 5000, SA, Australia*
[c] *Future Industries Institute, University of South Australia, Mawson Lakes, SA 5095, Australia*
[d] *Cleft & Craniofacial South Australia, Women's & Children's Hospital, Adelaide, Australia*
[e] *Skin Research Centre, York Biomedical Research Institute, Hull York Medical School, University of York, UK. E-mail: Miko.Yamada@hyms.ac.uk*
† Electronic supplementary information (ESI) available: Table S1 and supporting data. See DOI: https://doi.org/10.1039/d4tb02281e

This journal is © The Royal Society of Chemistry 2025

J. Mater. Chem. B, 2025, **13**, 6393–6401 | **6393**

matrix. Charge carriers in CP can delocalize within the extended π-bonded network, propagating along polymer chains and between neighbouring chains, thereby imparting conductivity to the polymer. PEDOT, in particular, has demonstrated superior stability and charge transport properties, leading to conductivities reaching up to 7600 S cm^{-1},[24] comparable to inorganic semiconductors such as silicon and germanium, as well as conductive materials like graphite.[25]

The recent growth of CPs has highlighted considerable interest in their integration into wearable and skin-attachable biomedical devices, owing to their high electrical conductivity, lightweight nature, mechanical flexibility and feasible fabrications.[26] The increasing use of CPs in wearable sensors is attributed to their efficient electron transfer at the bioelectronic interface and tunable conductivity.[27,28] Among these materials, PEDOT has emerged as a leading candidate due to its exceptional stability, high electrical conductivity, mechanical robustness, and suitability for biological interfaces.[29,30] PEDOT-coated MNs have shown significant potential for transdermal applications, demonstrating capabilities in both biosensing and drug delivery. Recent studies have shown that PEDOT-coated MNs can effectively penetrate the skin, enabling real-time monitoring of biomarkers such as pH in interstitial fluid with up to 93% accuracy compared to conventional probes.[31] The MNs showed minimal inflammatory response and high skin compatibility in porcine skin and live animal models. Moreover, PEDOT-based MNs demonstrated stable electrochemical impedance ($\sim$1.2 kΩ at 1 kHz) and consistent signal transduction in *ex vivo* skin models over extended wear durations as electrodes for wearable biosensing applications.[32] The MNs were tested on *ex vivo* porcine skin and *in vivo* rat models, demonstrating no cytotoxicity or adverse reactions. The application of PEDOT MNs in transdermal drug delivery enables controlled, pain-free administration of therapeutics, with studies in porcine skin demonstrating efficient drug diffusion ($\sim$85% release within 24 hours) and reliable penetration depths of approximately 500 μm, ensuring effective transdermal transport.[33] Additionally, PEDOT:PSS microneedles for continuous glucose monitoring were evaluated *in vivo* in rats, confirming no significant immune response or adverse skin effects,[34] indicating high biocompatibility of these PEDOT MNs.

Despite these promising attributes, a gap remains in evaluating the direct biocompatibility of PEDOT in human skin. Reported work on CPs performed on live human skin has shown no irritation to the subject's skin,[35] but these assessment were limited purely to surface observations. In addition, previous biocompatibility studies of CPs have been confined to *in vitro* experiments,[36] relying on the observation of specific cell growth in Petri dishes or animal models.[37,38] Though *in vitro* tests are the most common methods for cytotoxicity testing, with standard frameworks like ISO-10993-5 and ISO-10993-10 available,[39] they do not fully represent the complexity of human skin, which is composed of different layers and various cell types.[40] While the aforementioned animal studies have demonstrated the excellent biocompatibility of PEDOT MNs, they present translational limitations due to structural and biological

differences between animal and human skin.[41] Moreover, the use of animal models raises ethical concerns and may not fully capture human-specific responses to PEDOT MNs. To address this gap, this study evaluates the biocompatibility of PEDOT in excised human skin, providing a more direct and physiologically relevant assessment to inform its potential use in wearable biosensors.

Ex vivo biocompatibility assessments, particularly using human skin, provide a more accurate representation of *in vivo* conditions than *in vitro* or animal models. The viability of *ex vivo* human skin remains above 80% even after five days, providing a response that closely mimics *in vivo* conditions, *i.e.*, testing within a living person.[42] Hence, the presented work aimed to assess biocompatibility of CPs specifically in excised human skin, with a more detailed observation at the tissue and molecular levels. As such, MNs are suitable candidates as interfacing devices between CP and skin layers to enable transdermal biocompatibility interrogation, which to our knowledge, have never been reported in literature.

In this work, PEDOT coated MN is implanted in excised human skin, and after 24 hours incubation, the skin is evaluated based on (1) histopathological assessment of skin biopsy using histology and (2) gene expression of stress related gene markers using real-time polymerase chain reaction (RT-PCR) for tissue and molecular assessment. As previously mentioned, counterions doped in CPs are important in modifying the polymer's inherent properties but consequently affect polymer behaviour.[30] As such, in the RT-PCR experiments, two PEDOT derivatives, *i.e.* molecular tosylate (TOS) dopant in PEDOT:TOS and polymeric polystyrene sulfonate (PSS) dopant in PEDOT:PSS, are included.

2 Results and discussion

In this section, biocompatibility assessment on skin exposed to PEDOT coated MN are discussed, which include results from histology and RT-PCR. First, Fig. 1 shows procedures of the experiment. Details of each procedure are outlined in the methodology section.

2.1 Histology analysis on tissue

Histology is a method of studying the microscopic structure of tissues and is widely recognized for its ability to observe, detect and grade the severity of diseases.[43–45] Due to microscopic image of tissue obtained in histology image, it is particularly useful for assessing tissue damage and biocompatibility. For example, one report shows no adverse effect towards neuronal density for PEDOT/carbon fiber arrays.[46] Skin tissue was observed through histological images using H&E staining.[47] The histology analysis in Fig. 2 showed minimal to no adverse effects on skin morphology after 24 hours of exposure to PEDOT-coated MNs. This is supported by the low atypia scores in Fig. 3, where skin exposed to PEDOT-coated MNs has a score close to 0, indicating no obvious atypia. In contrast, the positive control has a score of 2, indicating severe atypia. The Cohen's kappa scores for inter-rater reliability between the assessors are above 0.80, indicating a high

6394 | *J. Mater. Chem. B*, 2025, **13**, 6393–6401

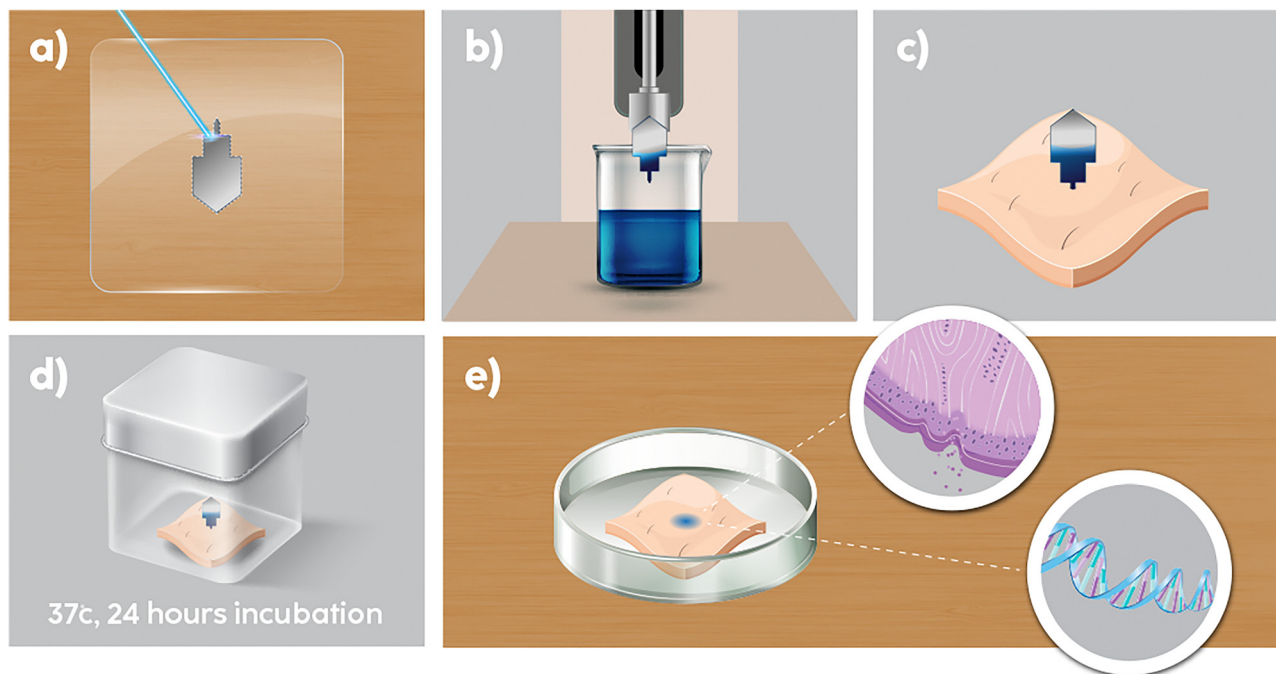This journal is © The Royal Society of Chemistry 2025

Fig. 1 Experimental procedures. (a) PMMA sheet laser cut into microneedle. (b) Microneedle tip dipped into PEDOTs solutions. (c) PEDOT coated microneedle tip is implanted into excised, fresh human skin. (d) Sample incubated in water bath at 37 deg for 24 hours. (e) Skin in contact with PEDOT coated MN was processed for histology and RT–PCR.
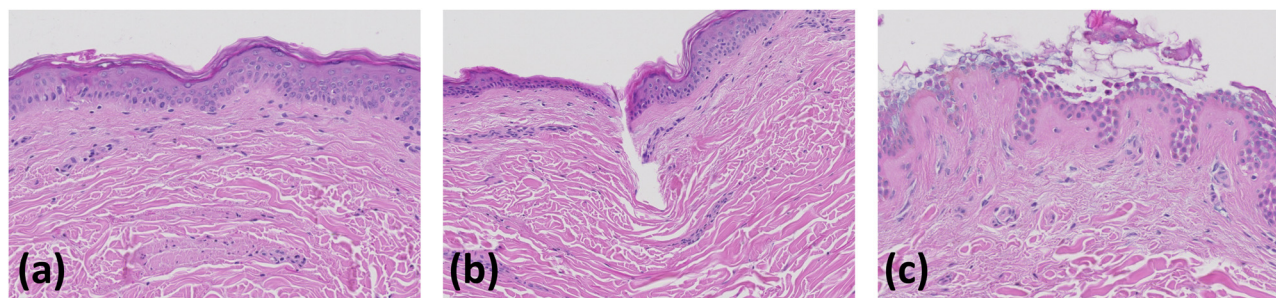

Fig. 2 Histology images for each treatment after 24 hours incubation. (a) Negative control – fresh skin (b) skin treated with PEDOT:PSS coated MN and (c) positive control – skin applied with 20% SDS.

level of agreement between them and demonstrating strong inter-rater reliability.
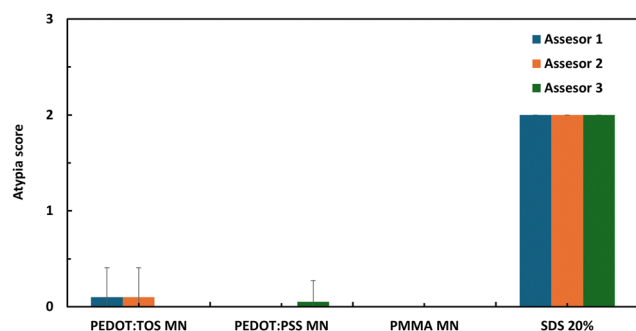

Fig. 3 Atypia scores on the skin samples after 24 hours incubation. (0 = no obvious atypia, 1-minimal atypia, 2 = severe atypia).

This suggests that PEDOT coatings, irrespective of the molecular or polymeric dopant, do not induce significant structural damage or pathological changes in human skin tissue. The minimal morphological changes observed, which were comparable to the negative control (uncoated MN), indicate a high degree of compatibility, with no significant inflammatory or degenerative responses. This outcome is crucial, as it demonstrates that PEDOT can be used in direct contact with human skin without causing irritation or damage, aligning with previous studies on CPs in other biological systems. The integration of histological evaluation and RT-PCR-based molecular stress markers in human *ex vivo* skin constitutes a more comprehensive approach compared to traditional cytotoxicity assays or *in vitro* cell models. This approach enables molecular-level insights into cellular stress responses that are not captured by histology alone, ensuring a more physiologically

This journal is © The Royal Society of Chemistry 2025

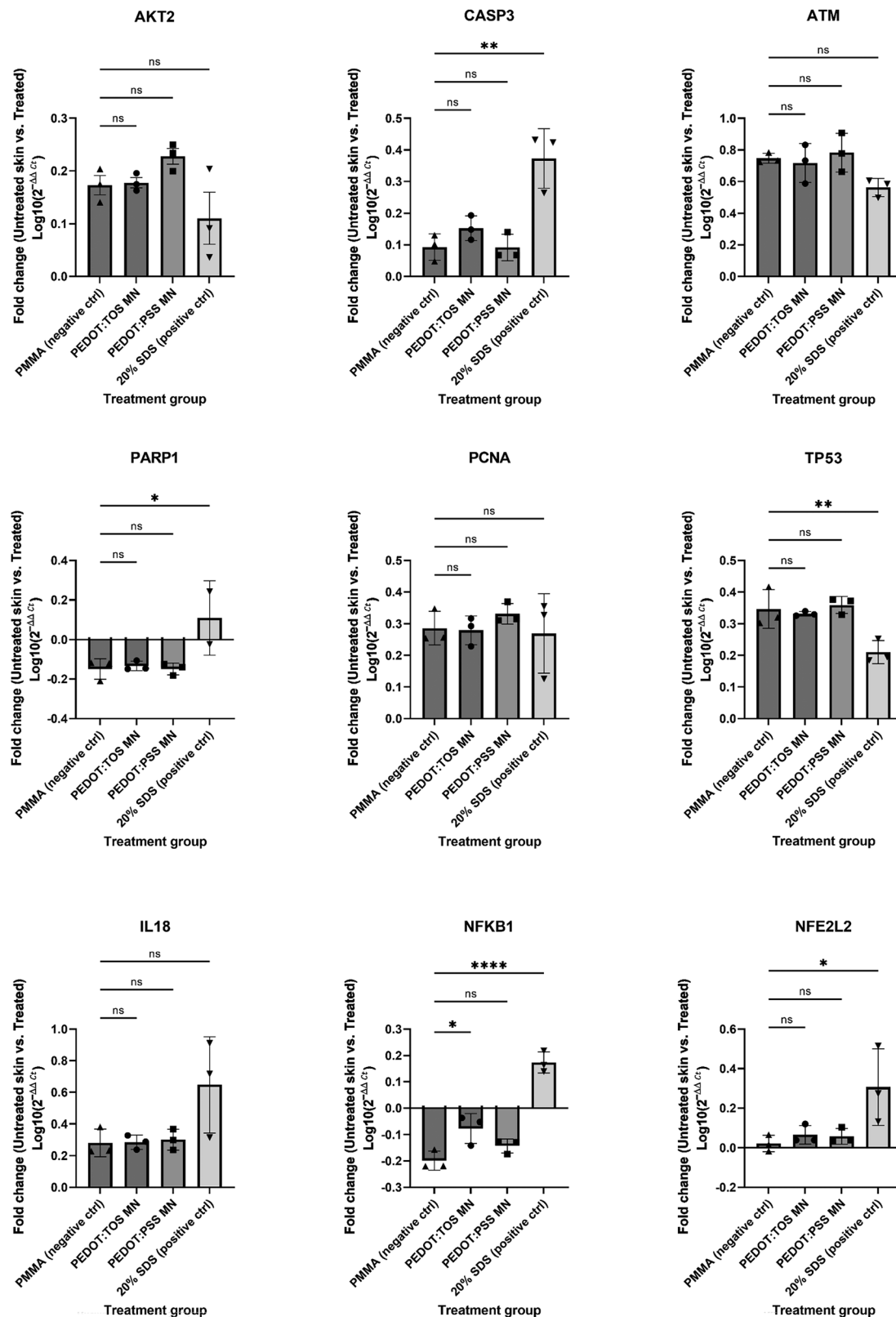*J. Mater. Chem. B*, 2025, **13**, 6393–6401 | **6395**

Fig. 4 Gene expression of related stress gene markers from RT-PCR. (a) AKT2 and (b) CASP3 to indicate cell's apoptosis, (c) ATM, (d) PARP1, (e) PCNA and (f) TP53 to indicate DNA damage followed by (g) IL18, (h) NFKB1 and (i) NFE2L2 to indicate inflammation and oxidative stress.

relevant evaluation of PEDOT-coated microneedles. This underscores the importance of thorough biocompatibility studies, particularly for materials widely claimed to be biocompatible without sufficient supporting evidence.

6396 | J. Mater. Chem. B, 2025, 13, 6393–6401

This journal is © The Royal Society of Chemistry 2025

2.2 Stress-related gene marker expression

Nucleic acids comprising double-stranded DNA and single-stranded RNA, carry the genomic information that governs cellular activities. In recent toxicology studies, gene expression levels of target genes, such as stress markers, are used to indicate cellular health. The function of quantitative real time PCR is to amplify and quantify the nucleic acid-based stress genes. In this work, TaqMan assay is adopted for RT-PCR owing to its high precision, excellent sensitivity and broad linear dynamic range inquantification.[48] The TaqMan assay uses a fluorogenic probe that is released upon completion of the target nucleic acid, and the increase in detectable fluorescence corresponds to the amount of PCR product, indicating gene expression levels. In this work, upon incubation with PEDOT coated MN, the skin was analyzed for gene expression of 18 stress related gene assays and 3 housekeeping genes. According to previous literature, these 18 genes are typically upregulated under cellular stress, hence they were measured to determine whether PEDOT induces stress responses at the molecular level in the skin.

The RT-PCR analysis of stress-related gene expression in human skin treated with PEDOT-coated microneedles (MN) illustrated in Fig. 4 revealed critical insights into cellular responses. Consistently, the treatment did not result in significant upregulation of genes selected for their association with cellular stress responses. This outcome suggests minimal perturbation at the molecular level and implies biocompatibility with human skin. A key observation was the differential expression of CASP3 and NFE2L2 between the PEDOT-treated groups and the positive control. CASP3, a gene involved in the execution phase of apoptosis, and NFE2L2, a master regulator of antioxidant response, were both significantly upregulated in the positive control group treated with 20% SDS, a known skin irritant. This upregulation confirms the sensitivity and reliability of the assay in detecting cellular stress responses. In contrast, these genes were not similarly induced in the PEDOT-treated groups, suggesting that PEDOT does not trigger significant apoptotic or oxidative stress pathways, thereby supporting its potential as a biocompatible material for microneedle applications.

Furthermore, IL18, a gene associated with inflammatory responses, exhibited a similar expression pattern. The PEDOT-treated MNs maintained expression levels similar to the negative control group, and all three groups exhibited lower levels than the SDS-treated positive control. This suggests the impact of PEDOT-coated microneedles on inflammatory pathways is less pronounced compared to stress induced by SDS. While the observed differences between the PEDOT-treated groups and the negative control were not statistically significant, the data suggest that PEDOT does not induce an inflammatory response comparable to that triggered by SDS, a known skin irritant. To ensure clarity, we acknowledge that our findings do not demonstrate statistically significant differences between the PEDOT-treated and negative control groups. Instead, the key observation is the absence of a significant upregulation of IL18 expression in PEDOT-treated samples, in contrast to the SDS-treated positive control, where a substantial increase was observed.

Interestingly, PARP1 and NFKB1 showed negative fold changes in the PEDOT-treated groups, with significant positive fold changes observed in the positive control when compared to the negative control. PARP1 is a key player in DNA repair, and its downregulation in PEDOT-treated samples suggests a reduction in DNA damage repair activity, which could be indicative of lower DNA damage induced by PEDOT. NFKB1, a critical regulator of inflammation and immune responses, also shows downregulated expression, implying reduced inflammatory signalling in response to PEDOT. The significant upregulation of these genes in the positive control further underscores the relative biocompatibility of PEDOT, as it appears to avoid the activation of pathways involved in DNA damage repair and inflammation.

Another significant finding was related to TP53, a central regulator of the DNA damage response. TP53 levels in PEDOT treatment groups were consistent with the negative control, which is not expected to induce a stress response. In contrast, the positive control showed significantly lower expression of TP53, which may reflect a stress response that dampens TP53 expression. A similar trend is also seen in AKT2, ATM and PCNA, genes involved in cell survival, DNA repair and proliferation respectively. These showed no significant changes in expression between treatment or control groups, which also supports the conclusion that PEDOT does not elicit a strong stress response.

To conclude, at the molecular level, RT-PCR analysis showed that the expression of stress-related gene markers did not significantly increase following exposure to PEDOT-coated MNs. Key markers of apoptosis (AKT2, CASP3), DNA damage (ATM, PARP1, PCNA, TP53), and inflammation/oxidative stress (IL18, NFKB1, NFE2L2) remained at baseline levels, suggesting that PEDOT does not induce significant cellular stress or damage. This molecular stability is critical for ensuring that wearable devices do not inadvertently activate stress pathways or lead to long-term damage when applied to the skin. The novel aspect of assessing the impact on stress-related gene markers offers a more comprehensive understanding of biocompatibility, providing crucial data that was previously lacking in the field.

The inclusion of both PEDOT:TOS and PEDOT:PSS in the study also allowed for a comparative evaluation of these materials. Both dopants exhibited similar biocompatibility profiles, though slight variations in gene expression levels were noted, which could be attributed to the different chemical properties of the dopants. Nevertheless, the differences were not substantial enough to indicate a preference for one over the other in terms of biocompatibility. This finding broadens the options for selecting the appropriate PEDOT formulation for specific applications, depending on other desired properties such as electrical conductivity or mechanical flexibility.

Collectively, these findings highlight that while PEDOT-coated microneedles may induce some changes in gene expression, these changes are generally mild and not indicative of a significant detrimental stress response. This makes them a promising candidate for biomedical applications, particularly in scenarios where minimising cellular stress and damage is

This journal is © The Royal Society of Chemistry 2025

J. Mater. Chem. B, 2025, **13**, 6393–6401 | **6397**

crucial such as transdermal drug delivery, biosensing, and other clinical applications.

3 Experimental

Medical grade PMMA sheet (0.25 mm thickness; Goodfellow) was used as substrate for all MN samples. Before being used, the substrate was sonicated in water and ethanol for 15 min and then treated with air plasma for 20 min (PDC-32G, Harrick Inc.) to increase surface adhesion with PEDOT coating.

3.1 Laser cutting to prepare PEDOT MNs

First, the MNs were designed in CorelDRAW Graphics Suite X6 (Corel, Canada) followed by laser cutting using LaserPro S290-20 laser etching system (GCC, Taiwan) with following parameters; 20% laser power, 7% speed, 3 passes with 2 mm thickness for minimal burning and clear cut.[49] The MN design consists of three sectional areas: (a) bulk, (b) neck, and (c) tip, as shown in Fig. S1 (ESI†). During skin incubation, only the tip area, which is coated with PEDOT, will be implanted within the skin.

3.2 Preparation of PEDOT:TOS MNs

The fabrication of PEDOT:TOS by vapor phase polymerization (VPP) followed the protocol described in previously published work.[30,50] First, an oxidant solution was prepared containing: 257 mM Fe(III) Tosylate (H. C. Starck as a 54 wt% solution in butanol -Baytron CB 40) and 58 mM triblock copolymer poly(ethylene glycol–propylene glycol–ethylene glycol) (PEG-PPG–PEG, M_w = 5800 g mol^{-1}, Sigma-Aldrich) in a 2.6:1 vol/vol mixture of ethanol to butanol as the solvent carrier. The PMMA MNs were dip-coated in the oxidant solution for 1 min and withdrawn at a rate of 50 mm min^{-1}. To remove excess solvent, samples were placed on a hotplate for 30 s at 70 °C before moving into the polymerization chamber (Binder Vacuum Oven-VD 115) for 1 hour at 23 °C and 45 mbar. The EDOT monomer was heated to 35 °C. Finally, samples were rinsed using ethanol and dried with low flow air gun to remove excess materials.

3.3 Preparation of PEDOT:PSS MNs

The fabrication of PEDOT:PSS followed protocols from previous works.[30,51] Poly(3,4-ethylenedioxythiophene)-poly(styrenesulfonate) (PEDOT:PSS, 1.3 wt% dispersion in H_2O, conductive grade, Sigma-Aldrich) was filtered through a 0.45 mm syringe filter to remove large aggregates. The PMMA MNs were dip-coated in PEDOT:PSS solution for 1 min and withdrawn at a rate of 50 mm min^{-1}. Samples were annealed at 70 °C for 30 min. To increase PEDOT:PSS conductivity and stability in water, the samples were treated in methanol by immersion for 15 min, then annealed on a hot plate at 70 °C for 5 min to remove excess methanol.

3.4 Incubation setup

Excised human skin from abdominoplasty was sourced from Calvary North Hospital, North Adelaide, Australia with consent from the participants and approval was obtained from University of South Australia, Research Ethic and Integrity (Protocol No:

2000745). Excess fat from skin was removed and the skin was cleaned before conducting the experiment soon after abdominoplasty procedure to ensure skin liveness. A 19 mm gauge syringe needle was used to make holes for the PEDOT coated MN to ensure the whole tip was implanted in the skin. For controls, uncoated PMMA MN was implanted in the skin as negative control and 20% concentration of sodium lauryl sulfate (SDS) (Sigma Aldrich) solution was applied on the skin as positive control. To prevent SDS evaporation into external environment, the applied area was enclosed using Franz cell and parafilm. Once all MNs and controls were set up, the skin was incubated in water bath at constant temperature of 35 degrees. After 24 hours incubation period, the skin was dissected for further analysis. The actual skin incubation setup is demonstrated in Fig. S2 (ESI†). Three different MN types namely PEDOT:TOS MNs, PEDOT:PSS MNs, and PMMA MNs (negative control) were implanted within the same skin sample, with replicates for each type placed within the same sample. This approach ensured that all MNs were exposed to the same biological environment, allowing for within-sample comparisons and minimizing inter-sample variability. Hence, differences observed could be attributed to MN composition rather than variations between skin samples.

3.5 RNA extraction

Once MN was removed, the implanted skin was cut using 3 mm biopsy punch. The skin was shredded into small pieces using a surgery knife and placed in RNAse-free beads lysis vessel (1.5 mL Eppendorf tubes prefilled with stainless steel beads, NextAdvance, USA). 350 μL of buffer RLT (Qiagen, German) was added to the tube. The tube was then placed in the bullet blender (NextAdvance_Lite bt12lt, USA) to disrupt skin with parameters of 90 s at speed 12. The tube was temporarily rested in ice for 5 s after each 30 s disruption to avoid excess heat from damaging the RNA. The supernatant, *i.e.* skin lysate was collected by pipetting and transferred to a new microcentrifuge tube. The lysate was centrifuged for 3 min at full speed to separate excess skin waste and the supernatant was again collected and transferred to a new microcentrifuge tube.

For RNA extraction, the RNeasy Mini kit (Qiagen. German) which included RNeasy mini spin column, buffer RLT, buffer RW1, buffer RPE and RNAse free water was used and performed according to the manufacturer's protocol. 1 volume of 70% ethanol* was added to the skin lysate and mixed immediately by pipetting. 700 μL of the mix sample was transferred including the precipitate into a RNeasy spin column, then centrifuged for 15 s at 10 000 rpm. Next, 350 μL buffer RW1 was added to the RNeasy spin column and centrifuged for 15 s at 10 000 rpm to wash the spin column membrane. DNase digestion was conducted to remove any DNA by adding DNase I incubation mix, *i.e.* 10 μL DNase I stock solution to 70 μL buffer RDD (RNase-Free DNase set, Qiagen, German) to tube and left at 20–30 °C for 15 min. 350 μL buffer RW1 was added to the RNeasy spin column and centrifuged for 15 s at 10 000 rpm. 500 μL buffer RPE was added to the RNeasy spin column and centrifuged for 15 s at 10 000 rpm to wash the spin column membrane and step was repeated with centrifugation for

6398 | *J. Mater. Chem. B*, 2025, **13**, 6393–6401

This journal is © The Royal Society of Chemistry 2025

2 min at same speed. The RNeasy spin column was placed in a new 2 mL collection tube and centrifuged at full speed for 1 min to eliminate any possible carryover. RNA on spin column was eluted by adding 30 μL RNAse-free water directly to the spin column membrane followed by centrifugation for 1 min at 10 000 rpm.

3.6 RNA quantity and quality assessment

The yield of RNA elution was determined by looking at quantity of the RNA using Qubit fluorometer (Invitrogen, Life Technology) and the quality of RNA using bioanalyzer (2100 Bioanalyzer, Agilent). In the former, RNA elution was added to Qubit RNA High Sensitivity (HS) Assay Kit according to manufacturing protocol and RNA concentration was read by Qubit (User Guide: Qubit RNA HS Assay Kits, MAN0002327). For the latter, RNA elution was added to RNA 6000 Nano kit (Agilent Technologies, California, USA) before read by Bioanalyzer. The RNA Integrity Number (RIN) was calculated in the provided software (2100 Expert Software).

3.7 Reverse transcription/cDNA synthesis

In RT-PCR, the amplification of DNA was counted instead of RNA. Hence, RNA was reverse transcribed to cDNA using reverse transcription Master Mix (Fluidigm, USA) following manufacturer's protocol. Mix of 1 μL reverse transcription (RT) Master Mix, 3 μL RNAse free water and 1 μL of RNA elution-referred to RT mix, was centrifuged and placed in thermal cycle for next step. First, the RT mix was incubated at 25 °C for 5 minutes to allow primer annealing. Next, RT mix was incubated at 42 °C for 30 minutes to allow cDNA synthesis. Finally, RT mix was incubated at 95 °C for 5 minutes to terminate the cDNA synthesis reaction. The quality of cDNA was determined using bioanalyzer (2100 Bioanalyzer, Agilent).

3.8 Real time PCR

Based on literature, several stress gene markers were selected, together with few housekeeping genes as listed in Table S1 (ESI†), using Taqman gene expression assay. Before conducting real-time PCR, the cDNA was preamplified to improve PCR amplification. For preamplification, the PreAmp Master Mix (Fluidigm, PN 1005580, South San Francisco, CA, USA) was used and performed according to the manufacturer's guidelines. For PCR, the 48.48 dynamic array TM IFC, assay loading reagent (Fluidigm, PN 85000736), GE sample loading reagent (Fluidigm, PN 85000735, 85000746) and the Master Mix (PerfeCTa® Fast Mix® II, low ROX, Quanta Biosciences, PN 95078-012, USA) were used. RT-PCR was performed according to the manufacturer's guidelines.

3.9 Quantification of stress gene expression

RNA input for reverse transcription to cDNA was normalised to 15.85 ng to ensure consistency across all samples and minimize variability in cDNA synthesis. Various cDNA samples from the study were pooled as a control sample for assay validation. Assays were included if they demonstrated a coefficient of determination (R^2) > 0.97 and efficiency of 80–120% on an 8

point, 2-fold standard curve. Assays were also required to test negative for product in a 4-point, 2-fold negative reverse transcriptase curve and in a no template control. RT-PCR reactions for each assay were performed in technical duplicate for each sample and the raw Ct values were provided by Epistem. This data was filtered using Python (v3.10.9) packages *numpy* and *pandas*. The service provider validated the limit-of-detection for the Fluidigm BioMark HD at the Ct value of 25, therefore reactions with values greater than this where excluded. Assay replicate values were filtered out if the Ct values varied by > 0.5 or if one of the replicate values was missing due to reaction failure. Where two or more independent experimental replicates (data for more than one skin donor) was removed due the filtering in a treatment group, assay data for that gene was discarded entirely. The assay technical replicate Ct values were averaged for the remaining data. The gene expression fold change between treated and untreated samples was calculated using the equation $2^{-\Delta\Delta Ct}$, where:

$$\Delta\Delta Ct = \Delta Ct_{\text{Treatment groups samples}} - \Delta Ct_{\text{Untreated control sample}},$$

$$(\Delta Ct_{\text{Treatment groups samples}} = Ct_{\text{Gene of interest in treatment sample}} - Ct_{\text{Geometric mean reference genes in treatment sample}}) \text{ and}$$

$$(\Delta Ct_{\text{Untreated group samples}} = Ct_{\text{Gene of interest in untreated sample}} - Ct_{\text{Geometric mean reference genes in untreated samples}})$$

Statistical analysis was performed in GraphPad Prism (v9.4.1). Prior to statistical analysis, the data was tested for normality and lognormality using the Shapiro-Wilk test. Not all gene data was normally distributed, therefore a non-parametric Kruskal–Wallis omnibus test was performed to find statistically significant differences between group means for each gene. A *post hoc* analysis was performed comparing groups to the PMMA MN negative control group using the Dunn's test ($\alpha = 0.05$).

3.10 Histology preparation

After 24-hour incubation, the skin was placed in tissue embedding cassette before it was immersed in neutral buffered 10% formalin solution (SigmaAldrich) for 15 hours for fixation and then transferred to 70% ethanol. Next, paraffin wax processing was performed on the tissue using Sakura Tissue-Tek VIP 6 Vacuum Infiltration Processor (Sakura Finetek, USA). Throughout the process, the tissue was immersed in ethanol 70%, 85%, 100% then Xylene followed by paraffin which completed in approximately 11 hours. Once finished, processed tissue was transferred to embedding station where the tissue was placed in the mould and filled with wax. After wax was set, the paraffin block was removed from the mould and ready for cutting.

The sectioning was conducted using Leica Rotary Microtome (Leica Microsystems Pty Ltd, Australia). Each block samples were cut into 5 μm thickness sections and placed on glass slides. For hematoxylin and eosin (H&E) staining, tissue section on glass slide was stained using Dako Coverstainer (Agilent Technologies). The automated staining process started with baking for 10 min and dipping in xylene, absolute ethanol, 70%

This journal is © The Royal Society of Chemistry 2025

J. Mater. Chem. B, 2025, **13**, 6393–6401 | **6399**

ethanol, hematoxylin (Dako Harris Haematoxylin, Agilent Technologies), acid alcohol, blue (Dako Bluing Buffer, Agilent Technologies), eosin (Dako Eosin Y Phyloxine B, Agilent Technologies) followed by drying for 10 min.

3.11 Histology evaluation

For histological analysis, PEDOT:PSS was selected as the representative sample due to its well-documented stability, aqueous processability, and extensive use in biomedical applications, in contrast to PEDOT:TOS. Additionally, PEDOT:TOS had lower visibility in tissue sections; hence, PEDOT:PSS was chosen to provide clear histological assessments. Ten slices from each skin sample were sent for histological assessment. Previously prepared stained sections of skin were analyzed by two dermatopathologists and one experienced scientist for identifying any morphological changes. The histological data was compared with positive and negative control and used for atypia scoring (0 = no obvious atypia, 1-minimal atypia, 2 = severe atypia) by PEDOT MN to determine its biocompatibility as implanted material in skin.

4 Conclusions

This study provides significant insights into the biocompatibility of PEDOT-coated MN when interfaced with human skin, a crucial factor for the development of wearable biosensors and therapeutic devices. The histology and RT-PCR analyses offer complementary perspectives, revealing that PEDOT, specifically in its TOS and PSS doped forms, interacts with skin tissue in a manner that supports its clinical and consumer healthcare applications. This is particularly relevant given the widespread use of these materials in biomedical devices, despite limited prior biocompatibility assessments. These findings established a solid foundation for the continued development of PEDOT-based wearable technologies, particularly for long-term applications in continuous health monitoring and therapeutic delivery. The high biocompatibility of PEDOT in human skin, as demonstrated in this study supports its use in a wide range of wearable and skin-interfacing devices. The ability of PEDOT-coated MNs to penetrate the skin and remain biocompatible for extended periods opens avenues for continuous monitoring and transdermal drug delivery applications. Moreover, the fact that no significant inflammatory response was observed reinforces the potential of PEDOT as a safe material. However, the 24-hour exposure period in this study provides only an initial indication of PEDOT's biocompatibility. Future research should explore longer exposure durations, additional stress markers and *in vivo* studies to fully validate the safety and efficacy of PEDOT in real-world applications.

Beyond the scope of this study, these findings contribute to the broader field of CPs in biomedical applications. The demonstration of PEDOT's compatibility with human skin at both tissue and molecular levels reinforces its viability for integration into next-generation biomedical devices. Additionally, this research addresses a critical gap in the literature by providing direct evidence of CP biocompatibility in human skin, which has previously been limited to *in vitro* and animal studies. By filling this gap, the study establishes a more rigorous standard for biocompatibility assessment.

Author contributions

Siti Musliha Ajmal Mokhtar: conceptualization, formal analysis, methodology, investigation, writing – original draft, and writing – review and editing. Nathalie J Nataren: formal analysis, methodology, writing – review and editing. Drew R Evans: conceptualization, funding acquisition, supervision, and writing – review and editing. Mark Moore: resources. Sofia MacHacaz: formal analysis and validation. Palmar Samuel Bradley: formal analysis and validation. Tarl W Prow: conceptualization, funding acquisition, supervision, and writing – review and editing. Miko Yamada: conceptualization, project administration, resources, supervision, validation, and writing – review and editing.

Data availability

The data supporting this article in Fig. 3 have been included as part of the ESI.† Data collected from human participants, described in Fig. 4, are not available for confidentiality reasons.

Conflicts of interest

There are no conflicts to declare.

Acknowledgements

References

1 Y. Yang and W. Gao, *Chem. Soc. Rev.*, 2019, **48**, 1465–1491.
2 J. A. Bunn, J. W. Navalta, C. J. Fountaine and J. D. Reece, *Int. J. Exerc. Sci.*, 2018, **11**, 503–515.
3 M. Dervisevic, M. Alba, B. Prieto-Simon and N. H. Voelcker, *Nano Today*, 2020, **30**, 100828.
4 S. T. Keene, D. Fogarty, R. Cooke, C. D. Casadevall, A. Salleo and O. Parlak, *Adv. Healthcare Mater.*, 2019, **8**, e1901321.
5 H. Mirzajani, T. Abbasiasl, F. Mirlou, E. Istif, M. J. Bathaei, C. Dag, O. Deyneli, D. Yazici and L. Beker, *Biosens. Bioelectron.*, 2022, **213**, 114450.
6 Y. Wang, I. R. Ausri, Z. Wang, C. Derry and X. S. Tang, *Sens. Actuators, B*, 2020, **308**, 127645.
7 S. A. Ventura, J. Heikenfeld, T. Brooks, L. Esfandiari, S. Boyce, Y. Park and G. B. Kasting, *Bioelectrochemistry*, 2017, **114**, 54–60.

6400 | *J. Mater. Chem. B*, 2025, **13**, 6393–6401

This journal is © The Royal Society of Chemistry 2025

8 A. R. Cardoso, M. H. de Sa and M. G. F. Sales, *Bioelectro-chemistry*, 2019, **130**, 107287.

9 Y. C. Chang, M. Soriano, R. A. Hahn, R. P. Casillas, M. K. Gordon, J. D. Laskin and D. R. Gerecke, *Toxicol. Appl. Pharmacol.*, 2018, **355**, 52–59.

10 Y. Qiao, J. Du, R. Ge, H. Lu, C. Wu, J. Li, S. Yang, S. Zada, H. Dong and X. Zhang, *Anal. Chem.*, 2022, **94**, 5538–5545.

11 G. Ma and C. Wu, *J. Controlled Release*, 2017, **251**, 11–23.

12 H. Teymourian, F. Tehrani, K. Mahato and J. Wang, *Adv. Healthcare Mater.*, 2021, **10**, e2002255.

13 N. Kashaninejad, A. Munaz, H. Moghadas, S. Yadav, M. Umer and N.-T. Nguyen, *Chemosensors*, 2021, **9**, 83.

14 J. J. García-Guzmán, C. Pérez-Ràfols, M. Cuartero and G. A. Crespo, *TrAC, Trends Anal. Chem.*, 2021, **135**, 116148.

15 J. Madden, C. O'Mahony, M. Thompson, A. O'Riordan and P. Galvin, *Sens. Bio-Sens. Res.*, 2020, **29**, 100348.

16 J. Yang, J. Yang, X. Gong, Y. Zheng, S. Yi, Y. Cheng, Y. Li, B. Liu, X. Xie and C. Yi, *Adv. Healthcare Mater.*, 2022, 2102547.

17 S. Anastasova, B. Crewther, P. Bembnowicz, V. Curto, H. M. Ip, B. Rosa and G. Z. Yang, *Biosens. Bioelectron.*, 2017, **93**, 139–145.

18 T. Zhao, C. Zheng, H. He, H. Guan, T. Zhong, L. Xing and X. Xue, *Smart Mater. Struct.*, 2019, **28**, 085015.

19 H. He, H. Zeng, Y. Fu, W. Han, Y. Dai, L. Xing, Y. Zhang and X. Xue, *J. Mater. Chem. C*, 2018, **6**, 9624–9630.

20 E. K. Varadharaj and N. Jampana, *J. Electrochem. Soc.*, 2016, **163**, B340–B347.

21 X. Qing, Y. Wang, Y. Zhang, X. Ding, W. Zhong, D. Wang, W. Wang, Q. Liu, K. Liu, M. Li and Z. Lu, *ACS Appl. Mater. Interfaces*, 2019, **11**, 13105–13113.

22 Y. Park, J. Jung and M. Chang, *Appl. Sci.*, 2019, **9**, 1070.

23 H. Shirakawa, E. J. Louis, A. G. MacDiarmid, C. K. Chiang and A. J. Heeger, *J. Chem. Soc., Chem. Commun.*, 1977, 578–580.

24 B. Cho, K. S. Park, J. Baek, H. S. Oh, Y.-E. Koo Lee and M. M. Sung, *Nano Lett.*, 2014, **14**, 3321–3327.

25 L. A. Fielding, J. K. Hillier, M. J. Burchell and S. P. Armes, *Chem. Commun.*, 2015, **51**, 16886–16899.

26 S. M. A. Mokhtar, E. Alvarez de Eulate, M. Yamada, T. W. Prow and D. R. Evans, *Med. Devices Sens.*, 2021, **4**, e10160.

27 S. Nambiar and J. T. Yeow, *Biosens. Bioelectron.*, 2011, **26**, 1825–1832.

28 T. M. Nguyen, S. Lee and S. B. Lee, *Nanomedicine*, 2014, **9**, 2263–2272.

29 Z. Rahimzadeh, S. Naghib, Y. Zare and K. Rhee, *J. Mater. Sci.*, 2020, **55**, 7575–7611.

30 S. M. Ajmal Mokhtar, E. Alvarez de Eulate, V. Sethumadhavan, M. Yamada, T. W. Prow and D. R. Evans, *J. Appl. Polym. Sci.*, 2021, **138**, 51314.

31 S. Odinotski, K. Dhingra, A. GhavamiNejad, H. Zheng, P. Ghavaminejad, H. Gaouda, D. Mohammadrezaei and M. Poudineh, *Small*, 2022, **18**, 2200201.

32 E. Shirzadi, M. Huynh, P. GhavamiNejad, H. Zheng, A. Saini, F. Bakhshandeh, F. Keyvani, D. Mantaila, F. A. Rahman, J. Quadrilatero, L. Soleymani and M. Poudineh, *Adv. Sens. Res.*, 2024, **3**, 2300122.

33 A. Keirouz, Y. Mustafa, J. Turner, E. Lay, U. Jungwirth, F. Marken and H. Leese, *Small*, 2023, **19**, 2206301.

34 P. GhavamiNejad, A. GhavamiNejad, H. Zheng, K. Dhingra, M. Samarikhalaj and M. Poudineh, *Adv. Healthcare Mater.*, 2023, **12**, 2202362.

35 X. Fu, W. Zeng, A. C. Ramirez-Perez and G. Lisak, *Chem. Commun.*, 2018, **54**, 980–983.

36 P. F. Hsiao, R. Anbazhagan, H. C. Tsai, K. Rajakumari, S. J. Lin, S. Y. Lin, K. Y. Lee, C. Y. Kao, R. S. Chen and J. Y. Lai, *Mater. Sci. Eng., C*, 2020, **107**, 110330.

37 R. Damalerio and M.-Y. Cheng, *Presented in part at the 2020 IEEE 70th Electronic Components and Technology Conference (ECTC)*, 2020.

38 S. C. Luo, E. Mohamed Ali, N. C. Tansil, H. H. Yu, S. Gao, E. A. Kantchev and J. Y. Ying, *Langmuir*, 2008, **24**, 8071–8077.

39 W. Li, J. Zhou and Y. Xu, *Biomed. Rep.*, 2015, **3**, 617–620.

40 Z. Zaidi and S. W. Lanigan, in *Dermatology in Clinical Practice*, ed. S. W. Lanigan and Z. Zaidi, Springer London, London, 2010, pp. 1–15, DOI: 10.1007/978-1-84882-862-9_1.

41 S. Ud-Din and A. Bayat, *Wound Repair Regen.*, 2017, **25**, 164–176.

42 S. Eberlin, M. S. D. Silva, G. Facchini, G. H. D. Silva, A. Pinheiro, S. Eberlin and A. D. S. Pinheiro, *ATLA, Altern. Lab. Anim.*, 2020, **48**, 10–22.

43 C. W. Elston and I. O. Ellis, *Histopathology*, 1991, **19**, 403–410.

44 K. Ishak, *J. Hepatol.*, 1995, **22**, 696–699.

45 D. E. Kleiner, E. M. Brunt, M. Van Natta, C. Behling, M. J. Contos, O. W. Cummings, L. D. Ferrell, Y. C. Liu, M. S. Torbenson and A. Unalp-Arida, *Hepatology*, 2005, **41**, 1313–1321.

46 P. R. Patel, H. Zhang, M. T. Robbins, J. B. Nofar, S. P. Marshall, M. J. Kobylarek, T. D. Kozai, N. A. Kotov and C. A. Chestek, *J. Neural. Eng.*, 2016, **13**, 066002.

47 H. J. Laubach, Z. Tannous, R. R. Anderson and D. Manstein, *Lasers Surg. Med.*, 2006, **38**, 142–149.

48 D. E. Watson and B. Li, *Int. J. Toxicol.*, 2005, **24**, 139–145.

49 S. M. A. Mokhtar, M. Yamada, T. W. Prow, M. Moore, X. L. Strudwick and D. R. Evans, *J. Mater. Chem. B*, 2023, **11**, 5021–5031.

50 S. Rudd, P. Desroches, E. Switalska, E. Gardner, M. Dalton, P. Buss, E. Charrault and D. Evans, *Sens. Actuators, B*, 2019, **281**, 582–587.

51 D. Alemu, H.-Y. Wei, K.-C. Ho and C.-W. Chu, *Energy Environ. Sci.*, 2012, **5**, 9662–9671.

This journal is © The Royal Society of Chemistry 2025

J. Mater. Chem. B, 2025, **13**, 6393–6401 | **6401**